

## Anomalous Coulomb Drag between InAs Nanowire and Graphene Heterostructures

Richa Mitra<sup>1</sup>, Manas Ranjan Sahu<sup>1</sup>, Kenji Watanabe<sup>2</sup>, Takashi Taniguchi<sup>2</sup>, Hadas Shtrikman<sup>3</sup>,  
A. K. Sood<sup>1</sup> and Anindya Das<sup>1,\*</sup>

<sup>1</sup>*Department of Physics, Indian Institute of Science, Bangalore 560012, India*

<sup>2</sup>*National Institute for Materials Science, Namiki 1-1, Ibaraki 305-0044, Japan*

<sup>3</sup>*Department of Physics, Weizmann Institute of Technology, Rehovot 7610001, Israel*



(Received 7 November 2019; accepted 21 February 2020; published 17 March 2020)

Correlated charge inhomogeneity breaks the electron-hole symmetry in two-dimensional (2D) bilayer heterostructures which is responsible for nonzero drag appearing at the charge neutrality point. Here we report Coulomb drag in novel drag systems consisting of a two-dimensional graphene and a one-dimensional (1D) InAs nanowire (NW) heterostructure exhibiting distinct results from 2D-2D heterostructures. For monolayer graphene (MLG)-NW heterostructures, we observe an unconventional drag resistance peak near the Dirac point due to the correlated interlayer charge puddles. The drag signal decreases monotonically with temperature ( $\sim T^{-2}$ ) and with the carrier density of NW ( $\sim n_N^{-4}$ ), but increases rapidly with magnetic field ( $\sim B^2$ ). These anomalous responses, together with the mismatched thermal conductivities of graphene and NWs, establish the energy drag as the responsible mechanism of Coulomb drag in MLG-NW devices. In contrast, for bilayer graphene (BLG)-NW devices the drag resistance reverses sign across the Dirac point and the magnitude of the drag signal decreases with the carrier density of the NW ( $\sim n_N^{-1.5}$ ), consistent with the momentum drag but remains almost constant with magnetic field and temperature. This deviation from the expected  $T^2$  arises due to the shift of the drag maximum on graphene carrier density. We also show that the Onsager reciprocity relation is observed for the BLG-NW devices but not for the MLG-NW devices. These Coulomb drag measurements in dimensionally mismatched (2D-1D) systems, hitherto not reported, will pave the future realization of correlated condensate states in novel systems.

DOI: [10.1103/PhysRevLett.124.116803](https://doi.org/10.1103/PhysRevLett.124.116803)

Correlated electronic states continue to be the focus of the condensed matter community, thanks to their rich complexity in physics and fascinating technological potential in the near future. Over the years the search for realizing highly correlated states has led to the discovery of novel many-body states like excitonic condensate states [1–4], fractional quantum Hall states [5,6], Luttinger liquid phase [7–10], etc. Coulomb drag has proven to be the quintessential tool for probing the electron-electron interaction in correlated systems and studied in a diverse set of systems like 2D electron gas (2DEG) based (AlGaAs/GaAs) heterostructures [1,2,4,11–14] to quantum wires [7–10]. In Coulomb drag, current ( $I_D$ ) passing in one of the layers produces an open circuit voltage ( $V_D$ ) in the other layer without any particle exchange. Very recently, graphene based heterostructures [15–19] have revealed intriguing feature of the drag signal at the Dirac point [15,17,18]; namely, that it can have both positive [15] and negative [18] amplitudes. A puzzling feature is its temperature dependence, which shows monotonic behavior with a maximum at the lowest temperature in BLG [18] whereas nonmonotonic variation with a maximum at an intermediate temperature ( $\sim 100$  K) for MLG [15]. The drag signal at the Dirac point

cannot be explained by the conventional momentum drag mechanism involving the momentum transfers from the drive to the drag layer; and hence two new mechanisms, namely, energy drag [20–22] and inhomogeneous momentum drag [23] have been proposed.

A new drag system consisting of 2D graphene and a confined 1D nanowire or nanotube not only has a potential for probing the graphene locally, but also the dimensionally mismatched Coulomb drag system can potentially become the foreground for studying the effect of dimension on scattering mechanisms in Coulomb drag [39–41]. This kind of drag system is expected to show novel quantum phases in the strong coupling regime [42] in addition to being a tool for studying the graphene hydrodynamics near the Dirac point [43]. With this motivation we have carried out the Coulomb drag experiments in MLG-InAs NW and BLG-InAs NW devices as a function of density ( $n$ ), temperature ( $T$ ), and magnetic field ( $B$ ). The MLG-NW devices show a drag resistance ( $R_D = V_D/I_D$ ) maximum around the Dirac point and its dependence on  $n$ ,  $T$ , and  $B$  establish the energy drag as the dominant mechanism. In comparison, absence of the drag signal at the Dirac point for the BLG-NW devices and flipping sign across the Dirac

point with negligible dependence on  $T$  and  $B$  suggest the dominance of the momentum drag mechanism.

The device and measurement configuration are schematically presented in Fig. 1(a). All the devices comprise of heterostructures of hexagonal boron nitride (hBN) encapsulated graphene stack and InAs NW with diameter between 50 to 70 nm. The heterostructures were assembled by the standard hot pick up technique [44,45], where the  $\sim 10$  nm thick top hBN of the graphene stack separates the graphene channel and the NW (SI-1 of the Supplemental Material [24]). The inhomogeneity ( $\delta n$ ) of graphene is  $\sim 2.5 \times 10^{10} / \text{cm}^2$ , which corresponds to a Fermi energy broadening of  $\Delta_0 \sim 15$  and  $\sim 0.5$  meV for MLG and BLG, respectively. The NWs could only be electron doped due to Fermi energy pinning near the conduction band. The 1D nature of the NW used is ascertained by measuring the electrical conductance as a function of the  $V_{\text{BG}}$  for shorter channel length showing participation of 3–5 subbands (see SI-1E of the Supplemental Material [24]). The charge inhomogeneity in the NW was investigated by measuring the temperature-dependent conductance as shown in Fig. S-1F of the Supplemental Material [24], which suggests the localization length of  $\sim 100$ – $200$  nm. All the measurements were done in a He4 cryostat in the temperature range of 1.5 to 200 K.

The drag measurements were performed by the dc technique, where  $I_D$  was passed through the graphene

and  $V_D$  was measured on the NW as shown in Fig. 1(a) or vice versa. The carrier density of the graphene ( $n_G$ ) and NWs ( $n_N$ ) were tuned by the  $\text{SiO}_2$  back gate ( $V_{\text{BG}}$ ) and by a voltage ( $V_{\text{GR}}$ ) between the graphene and the NW (SI-2 of the Supplemental Material [24]). In our dc measurements, the drag signal contains a predominant flipping component (sign reversal of the drag voltage with  $I_D$ ) together with a small nonflipping component. Here, we present the extracted flipping part (in the linear regime) as mentioned in Sec. SI-2B of the Supplemental Material [24], which is consistent with the drag signal measured by the low-frequency ac (at 7 Hz) technique (SI-2 of the Supplemental Material [24]). The tunneling resistance of the  $\sim 10$  nm thick hBN between the graphene and NWs was more than 5–10  $G\Omega$  in all the devices. We have used two MLG-NW (D1, D2) and two BLG-NW (D3, D4) devices for the drag measurements.

Figure 1(b) shows the 2D color map for the MLG-NW device (D1) at  $T = 1.5$  K and  $n_N \sim 4 \times 10^5 \text{ cm}^{-1}$ , where  $R_D$  is plotted with  $I_D$  varying from  $-10$  to  $+10 \mu\text{A}$  and  $n_G$  varying from 0 to  $2 \times 10^{11} / \text{cm}^2$  for both electron and hole doping. The drag signal peaks near the Dirac point and subsequently decays at higher  $n_G$ . Figure 1(c) shows  $R_D$  at different temperatures. The peak magnitude decreases rapidly with temperature as shown by open circles in Fig. 1(e). Figure 1(d) shows the dependence of  $R_D$  on magnetic field up to 400 mT at  $T = 1.5$  K. Notably, we

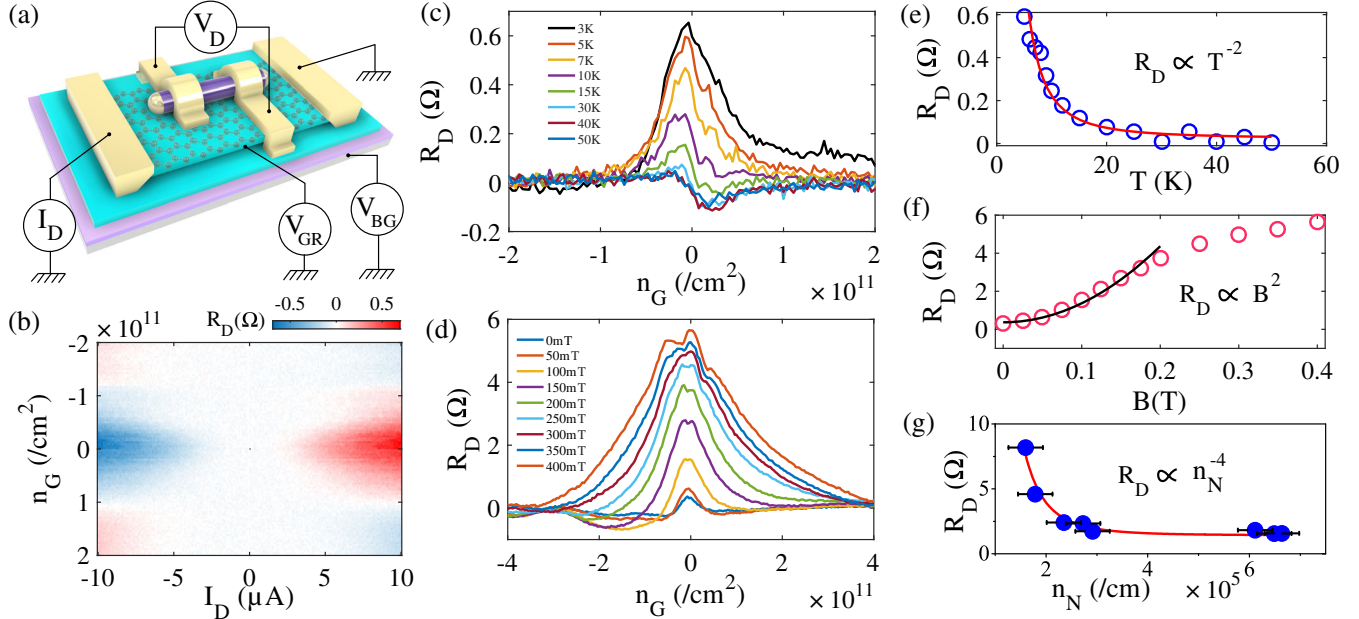


FIG. 1. (a) Device schematic: The heterostructure consists of an InAs nanowire on top of a hBN encapsulated graphene stack assembled on Si/SiO<sub>2</sub> substrate. (b) 2D color map of  $R_D$  at  $T = 1.5$  K plotted against the  $I_D$  and  $n_G$  for the D1 device (MLG-NW). (c) Response of the  $R_D$  at different temperatures. (d)  $R_D$  versus  $n_G$  plot for different magnetic fields at  $T = 1.5$  K. (e) Peak values of the  $R_D$  (blue circles) plotted with temperature.  $R_D$  decreases with temperature and fits (red solid line) well with  $R_D \propto T^{-2}$ . (f) The pink open circles are the peak value of  $R_D$  plotted with magnetic field at  $T = 1.5$  K. The black solid line shows data up to 200 mT fits well with  $B^2$ . (g)  $R_D$  at the Dirac point as a function of  $n_N$  at  $T = 1.5$  K. The solid line is an overlay of  $n_N^{-4}$  with the data. The error bars in  $n_N$  have been estimated from different sweeps of measurements of the device shown in Fig. S-3B (a) of the Supplemental Material [24].

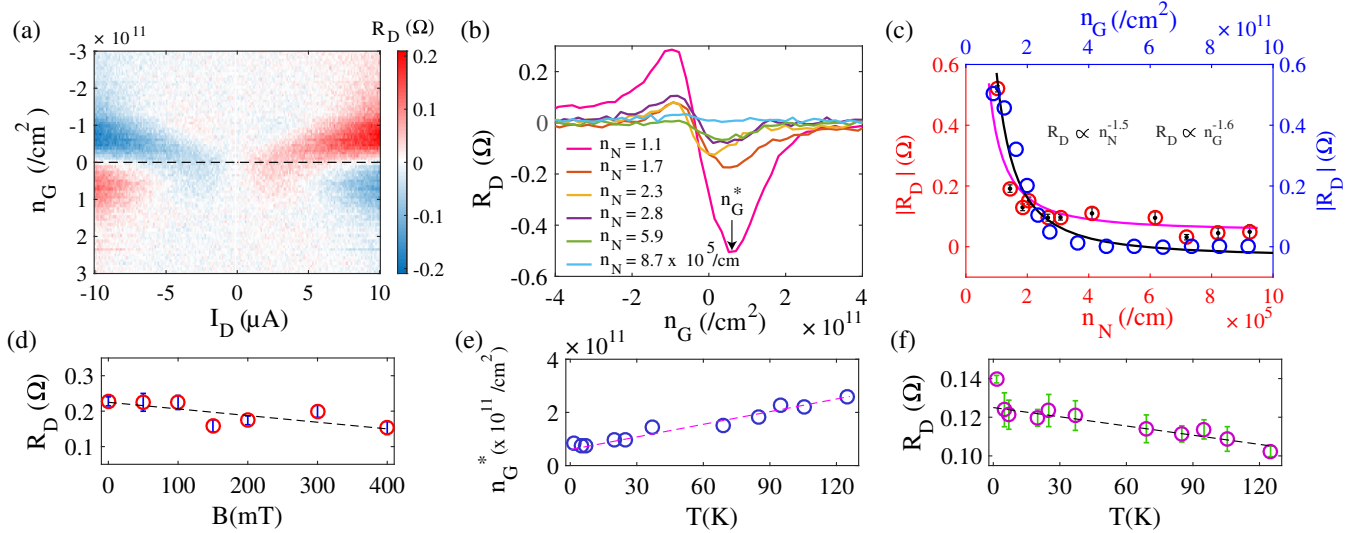


FIG. 2. (a) 2D color map of  $R_D$  with  $I_D$  and  $n_G$  at  $T = 1.5$  K,  $V_{GR} = 1$  V for a BLG-NW device. The horizontal dashed line is the Dirac point of the graphene. (b)  $R_D$  versus  $n_G$  plot at  $T = 1.5$  K for different  $n_N$  tuned by the  $V_{GR}$  from 0.9 to 5 V. (c) The red circles are the plot for dip value of  $R_D$  at different  $n_N$ . The variation of the drag signal with  $n_G$  at  $V_{GR} = 0.9$  V is indicated by the blue open circles. The solid lines are the fitting to  $\sim n_N^{-1.5}$  and  $n_G^{-1.6}$ . (d) The variation of  $R_D$  with magnetic field at  $T = 1.5$  K. (e) The position of the dip ( $n_G^*$ ) of  $R_D$  as a function of temperature (raw data in Fig. S-4B of the Supplemental Material [24]). (f) The dip value of  $R_D$  plotted as a function of temperature. The dashed lines in (d), (e), and (f) are the guiding lines.

observe a giant increase (by 1 order of magnitude) of the drag peak with increasing magnetic field as shown by open circles in Fig. 1(f). The dependence of the drag peak on  $n_N$  measured by varying  $V_{GR}$  (SI-3C of the Supplemental Material [24]) is shown in Fig. 1(g).

Figure 2(a) shows the 2D color map for the BLG-NW device (D3), where  $R_D$  is plotted as a function of  $I_D$  and  $n_G$  at  $T = 1.5$  K for  $n_N \sim 1.3 \times 10^5 \text{ cm}^{-1}$ . In contrast to MLG-NW devices, the drag signal flips sign from positive to negative as  $n_G$  shifts from holes to electrons across the Dirac point with distinct peak and dip at finite densities of holes and electrons. At the Dirac point the  $R_D$  is negligible unlike the MLG-NW device. Figure 2(b) shows  $R_D$  as a function of  $n_G$  for different NW densities ( $n_N \sim 1$  to  $10 \times 10^5 \text{ cm}^{-1}$ ) tuned by  $V_{GR}$ . The blue circles in Fig. 2(c) quantify how the magnitude of  $R_D$  decreases with  $n_G$  [for electron side in Fig. 2(b)] for  $n_N = 1.1 \times 10^5 \text{ cm}^{-1}$ , whereas the red circles show the magnitude of the dip of  $R_D$  at  $n_G^*$  [marked in Fig. 2(b)] as a function of  $n_N$ . Figure 2(d) shows that  $R_D$  at  $n_G^*$  for the BLG-NW device remains almost constant with magnetic field (raw data in SI-4A of the Supplemental Material [24]), in contrast with the MLG-NW device. Figures 2(e) and 2(f) demonstrate the temperature dependence of the drag signal for the BLG-NW device. It can be seen from the Supplemental Material [24] Fig. S-4B (raw data) that the peak (hole side) or dip (electron side) position of  $R_D$  shifts towards higher carrier density in graphene with increasing temperature for a fixed carrier density of the NW ( $n_N \sim 1 \times 10^5 \text{ cm}^{-1}$ ). Figure 2(e) shows the position ( $n_G^*$ ) and the corresponding value of  $R_D$  in Fig. 2(f) as a function

of temperature. Unlike the MLG-NW device, the drag signal in the BLG-NW device clearly displays much less variation with temperature.

The observations of monotonic decrease of drag signal of the MLG-NW device as well as weak dependence of the drag signal of the BLG-NW device on increasing temperature are anomalous as compared to the conventional momentum drag which predicts a  $T^2$  [46–49] increase as seen in double-layer MLG heterostructures [15]. Anomaly in temperature dependence, specifically, drag signal increasing with lowering temperature has been observed in 2DEG (GaAs-AlGaAs) [11] or 2DEG-graphene [19] heterostructures. The anomalous upturn of the drag signal with lowering temperature at low temperature regime indicated the presence of interlayer excitonic condensation in 2DEG-graphene system [19] or the Luttinger liquid state in quantum wire systems [7]. The possibility of excitonic condensation in our MLG-NW devices is ruled out as the drag peak appears at the Dirac point of graphene with the NW having a finite density.

To explain our results, we first recall the three main mechanisms of the Coulomb drag: (i) homogeneous momentum drag (HMD)—momentum transfers via Coulomb mediated scattering, (ii) inhomogeneous momentum drag (IMD)—momentum transfer in presence of correlated inter-layer charge puddles and (iii) energy drag (ED)—vertical energy transfer in presence of correlated interlayer charge puddles. Since the HMD signal should be zero at the Dirac point and increases as  $T^2$  in a Fermi liquid [46–49], it can be ruled out as the possible mechanism for our MLG-NW devices. Now, both IMD and energy drag

mechanisms predict a maximum of  $R_D$  at the Dirac point due to the presence of correlated interlayer charge puddles, although the underlying physics is different. The effective momentum theory (EMT) of IMD [23] suggests an increase of the drag signal with temperature in the low temperature regime and should decrease when  $k_B T > 0.5\Delta_0$ . Further, the EMT does not explain the effect of magnetic field on the drag signal. Thus the anomalous decrease with temperature and enhancement of  $R_D$  with magnetic field in our MLG-NW devices is not consistent with the predictions of the IMD.

Coming now to the energy drag mechanism, a positive correlation of charge inhomogeneities in MLG and NW gives rise to a positive drag peak around the Dirac point due to the combined effect of Coulomb mediated vertical energy transfer and the thermoelectric Peltier effect [20]. The energy drag is expected to increase [22] with magnetic field as  $B^2$  and display a nonmonotonic behavior with temperature [20]. Figure 1(f) for the MLG-NW device clearly shows  $B^2$  dependence of  $R_D$  at lower magnetic field which is consistent with the energy drag mechanism [20]. To explain the temperature dependence, a quantitative theory of ED in 2D-1D system is required. In the absence of such theory, we appeal to Song *et al.* for a 2D-2D system which shows [20]  $R_D \propto (1/2T\kappa)(\partial Q/\partial\mu_G)(\partial Q/\partial\mu_N)$ , where  $\partial Q/\partial\mu$  is the partial derivatives of the Peltier coefficient  $Q$  with respect to the chemical potentials of drive ( $\mu_G$ ) and drag layers ( $\mu_N$ ). The quantity  $\kappa$  is the sum of the thermal conductivities ( $\kappa_G + \kappa_N$ ) of the two layers. For double-layer graphene heterostructures, the energy drag mechanism [20] generates a nonmonotonic temperature behavior where the drag signal increases as  $T^2$  up to a temperature equivalent to  $\sim\Delta_0$  and subsequently decreases as  $T^{-4}$ . For the MLG-NW devices, the typical value of  $\Delta_0$  is  $\sim 15$  meV (equivalent to 150 K). Hence, according to the energy drag mechanism, the drag signal should have increased monotonically up to  $\sim 150$  K. While discussing the energy drag mechanism, we need to keep in mind that the studies so far assume two identical layers of graphene having similar properties such as mobility, thermal conductivity, electrical conductivity, etc. In contrast, we measure the Coulomb drag between two very dissimilar systems: a high mobility 2D graphene sheet and a low-mobility semiconducting 1D NW, with very different electrical transports. More importantly, the NWs have electrical conductivity  $\sim 1e^2/h$  and thus poor electronic thermal conductivity ( $\kappa_e$ ) as compared to graphene, making phonon contributions to the thermal transport ( $\kappa_{ph}$ ) dominant [50]. Hence,  $\kappa = \kappa_G + \kappa_N = \kappa_e + \kappa_{ph}$ . Since  $\kappa_e \propto T$  and  $\kappa_{ph}$  (electron-phonon contribution)  $\propto T^5$  (Refs. [51,52]),  $\kappa = (aT + bT^5)$ , where  $a$  and  $b$  are the relative contributions from the electronic and the phononic parts. The contribution of the interlayer dielectric hBN to  $\kappa_{ph}$  is expected to be much smaller than that of the NW and hence is not expected to affect the temperature dependence.

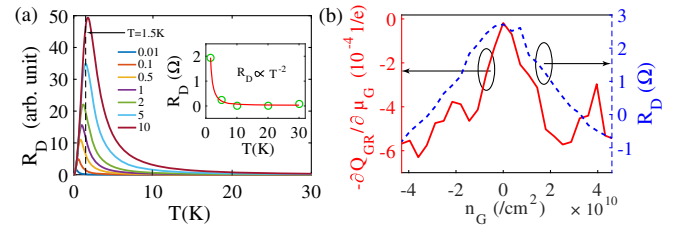


FIG. 3. (a) Theoretically calculated  $R_D$  as a function of temperature for several values of  $a/b$  ranging from 0.01 to 10. The inset shows the experimental  $R_D$  (open circles) as a function of temperature for D2 device with  $T^{-2}$  fitting (solid red line). (b) Similarities between  $\partial Q/\partial\mu$  (red solid line) and  $R_D$  (blue dashed line).

Using  $(\partial Q/\partial\mu_G) \propto (T^2/\Delta_0^2)$  at the Dirac point and  $(\partial Q/\partial\mu_N) \propto T^2/\mu_N^2$  at  $\mu_N \neq 0$  (SI-5 of the Supplemental Material [24] for details), the temperature dependence of  $R_D$  is  $R_D \propto \{T^3/[\mu_N^2\Delta_0^2(aT + bT^5)]\}$ . Noticeably, the  $R_D$  still has the nonmonotonic dependence on temperature, depending on the relative magnitudes of the parameters  $a$  and  $b$ . The calculated  $R_D$  for different values of  $a/b$  is shown in Fig. 3(a), where one can see that the crossover happens at temperatures near  $\sim 1$  K (below our temperature range) and decreases as  $T^{-2}$  consistent with our experimental data [the solid lines in Fig. 1(e) for D1, and in the inset of Fig. 3(a) for D2]. Furthermore, Fig. 3(b) shows the similarities between the dependence of  $R_D$  and  $\partial Q/\partial\mu_G$  on  $n_G$  (SI-5 of the Supplemental Material [24]), which further strengthens the energy drag to be the dominant mechanism in MLG-NW devices. Moreover, the effect of carrier density of the NW on the drag peak showing  $n_N^{-4}$  dependence [Fig. 1(g)] is compatible with the energy drag mechanism as the  $(\partial Q/\partial\mu_N) \propto (T^2/\mu_N^2) = (T^2/n_N^4)$  (SI-5 of the Supplemental Material [24]).

We will now discuss the possible drag mechanism for the BLG-NW devices. Drag being almost zero near the Dirac point [Figs. 2(a) and 2(b)] rules out energy drag and IMD, in favor of HMD as a possible mechanism, where  $R_D \propto [(k_B T)^2/n_G^{1.5}n_N^{1.5}]$  is consistent with our result as shown in Fig. 2(c) (solid lines). However, we do not observe the predicted  $T^2$  increase of the drag signal [Fig. 2(f)]. This can be due to that the drag signal not only slowly varies with increasing temperature but also the shift of the  $R_D$  maximum and minimum position ( $n_G^*$ ) towards higher  $n_G$  [Figs. 2(e) and 2(f)]. This happens due to the temperature-induced Fermi energy broadening, over and above the intrinsic disorder limited  $\Delta_0$  ( $\sim 0.5$  meV in BLG).

In order to see the effect of dimensionality mismatch on the Onsager reciprocity relation, we have measured the drag signal in both NW and graphene as shown in Fig 4. As can be seen, the Onsager relation is valid in the BLG-NW device [Fig. 4(b)], whereas it is violated for the MLG-NW device [Fig. 4(a)]. The violation of the Onsager relation has been reported in bilayer 2DEG and 2DEG-graphene

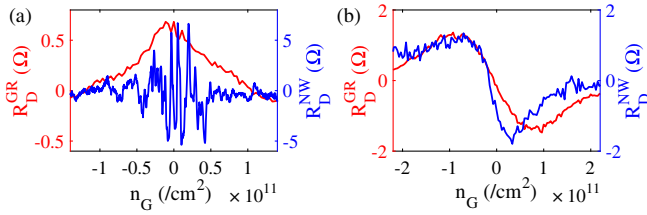


FIG. 4. (a) Onsager in MLG-NW device at  $T = 1.5$  K. The red line corresponds to the  $R_D$  measured on NW whereas the blue line corresponds to the  $R_D$  measured on MLG. (b) Similar data for the BLG-NW device.

devices [2,14,19], but the exact reason is not clearly understood. We suggest that the role of different drag mechanisms in the Onsager relation can be at play in the dimensionality mismatched devices.

In conclusion, we have performed drag measurements on dimensionally mismatched MLG/BLG-InAs NW heterostructures hitherto not reported. We observe very different drag signals for the MLG-NW and the BLG-NW devices. The MLG-NW devices show a maximum of  $R_D$  at the Dirac point and the peak value decreases with increasing temperature as well as with the carrier density of the NW. Further, the drag increases by 1 order of magnitude with magnetic field. These results show that the energy drag mechanism is dominant for the Coulomb drag in the MLG-NW heterostructures, where the phononic thermal conductivity of the NWs plays a significant role in reduced drag signal with increasing temperature. In contrast, for the BLG-NW devices, the drag reverses sign across the Dirac point as expected from the momentum drag mechanism, with slow variation with temperature and magnetic field. Our results are promising for realizing the correlated states in dimensionally mismatched novel devices, with different mechanisms at play.

Authors thank Dr. Derek Ho and Professor Shaffique Adam for providing the computational codes for inhomogeneous momentum drag. A.D. thanks DST (DSTO-2051) and acknowledges the Swarnajayanti Fellowship of the DST/SJF/PSA-03/2018-19. A. K. S. thanks Year of Science Fellowship from DST for the financial support. K.W. and T.T. acknowledge support from the Elemental Strategy Initiative conducted by the MEXT, Japan and the CREST (JPMJCR15F3), JST. We acknowledge Michael Fourmansky for his professional assistance in NWs MBE growth. H.S. acknowledges partial funding by Israeli Science Foundation (Grants No. 532/12 and No. 3-6799), BSF Grant No. 2014098 and IMOS-Tashtiot Grant No. 0321-4801. H.S. is an incumbent of the Henry and Gertrude F. Rothschild Research Fellow Chair.

\* anindya@iisc.ac.in

[1] M. Kellogg, I. B. Spielman, J. P. Eisenstein, L. N. Pfeiffer, and K. W. West, *Phys. Rev. Lett.* **88**, 126804 (2002).

- [2] J. A. Seamons, C. P. Morath, J. L. Reno, and M. P. Lilly, *Phys. Rev. Lett.* **102**, 026804 (2009).
- [3] J. Li, T. Taniguchi, K. Watanabe, J. Hone, and C. Dean, *Nat. Phys.* **13**, 751 (2017).
- [4] D. Nandi, A. Finck, J. Eisenstein, L. Pfeiffer, and K. West, *Nature (London)* **488**, 481 (2012).
- [5] J. P. Eisenstein, G. S. Boebinger, L. N. Pfeiffer, K. W. West, and S. He, *Phys. Rev. Lett.* **68**, 1383 (1992).
- [6] Y. W. Suen, L. W. Engel, M. B. Santos, M. Shayegan, and D. C. Tsui, *Phys. Rev. Lett.* **68**, 1379 (1992).
- [7] D. Laroche, G. Gervais, M. Lilly, and J. Reno, *Science* **343**, 631 (2014).
- [8] P. Debray, V. Zverev, O. Raichev, R. Klesse, P. Vasilopoulos, and R. Newrock, *J. Phys. Condens. Matter* **13**, 3389 (2001).
- [9] M. Yamamoto, M. Stopa, Y. Tokura, Y. Hirayama, and S. Tarucha, *Science* **313**, 204 (2006).
- [10] K. Flensberg, *Phys. Rev. Lett.* **81**, 184 (1998).
- [11] P. M. Solomon, P. J. Price, D. J. Frank, and D. C. La Tulipe, *Phys. Rev. Lett.* **63**, 2508 (1989).
- [12] T. J. Gramila, J. P. Eisenstein, A. H. MacDonald, L. N. Pfeiffer, and K. W. West, *Phys. Rev. Lett.* **66**, 1216 (1991).
- [13] M. Kellogg, J. P. Eisenstein, L. N. Pfeiffer, and K. W. West, *Phys. Rev. Lett.* **90**, 246801 (2003).
- [14] A. F. Croxall, K. Das Gupta, C. A. Nicoll, M. Thangaraj, H. E. Beere, I. Farrer, D. A. Ritchie, and M. Pepper, *Phys. Rev. Lett.* **101**, 246801 (2008).
- [15] R. Gorbachev, A. Geim, M. Katsnelson, K. Novoselov, T. Tudorovskiy, I. Grigorieva, A. H. MacDonald, S. Morozov, K. Watanabe, T. Taniguchi *et al.*, *Nat. Phys.* **8**, 896 (2012).
- [16] S. Kim, I. Jo, J. Nah, Z. Yao, S. K. Banerjee, and E. Tutuc, *Phys. Rev. B* **83**, 161401(R) (2011).
- [17] J. I. A. Li, T. Taniguchi, K. Watanabe, J. Hone, A. Levchenko, and C. R. Dean, *Phys. Rev. Lett.* **117**, 046802 (2016).
- [18] K. Lee, J. Xue, D. C. Dillen, K. Watanabe, T. Taniguchi, and E. Tutuc, *Phys. Rev. Lett.* **117**, 046803 (2016).
- [19] A. Gamucci, D. Spirito, M. Carrega, B. Karmakar, A. Lombardo, M. Bruna, L. Pfeiffer, K. West, A. C. Ferrari, M. Polini *et al.*, *Nat. Commun.* **5**, 5824 (2014).
- [20] J. C. W. Song and L. S. Levitov, *Phys. Rev. Lett.* **109**, 236602 (2012).
- [21] J. C. W. Song, D. A. Abanin, and L. S. Levitov, *Nano Lett.* **13**, 3631 (2013).
- [22] J. C. W. Song and L. S. Levitov, *Phys. Rev. Lett.* **111**, 126601 (2013).
- [23] D. Y. Ho, I. Yudhistira, B. Y.-K. Hu, and S. Adam, *Commun. Phys.* **1**, 41 (2018).
- [24] See Supplemental Material at <http://link.aps.org/supplemental/10.1103/PhysRevLett.124.116803> for addition raw data and detailed discussion on device fabrication, measurement techniques and analysis which includes Refs. [25–38].
- [25] K. S. Novoselov, A. K. Geim, S. V. Morozov, D. Jiang, Y. Zhang, S. V. Dubonos, I. V. Grigorieva, and A. A. Firsov, *Science* **306**, 666 (2004).
- [26] D. Purdie, N. Pugno, T. Taniguchi, K. Watanabe, A. C. Ferrari, and A. Lombardo, *Nat. Commun.* **9**, 5387 (2018).
- [27] A. Das, Y. Ronen, Y. Most, Y. Oreg, M. Heiblum, and H. Shtrikman, *Nat. Phys.* **8**, 887 (2012).

- [28] H. Shtrikman, R. Popovitz-Biro, A. V. Kretinin, and P. Kacman, *IEEE J. Sel. Top. Quantum Electron.* **17**, 922 (2010).
- [29] D. Suyatin, C. Thelander, M. Björk, I. Maximov, and L. Samuelson, *Nanotechnology* **18**, 105307 (2007).
- [30] C. R. Dean, A. F. Young, I. Meric, C. Lee, L. Wang, S. Sorgenfrei, K. Watanabe, T. Taniguchi, P. Kim, K. L. Shepard *et al.*, *Nat. Nanotechnol.* **5**, 722 (2010).
- [31] M. R. Sahu, P. Raychaudhuri, and A. Das, *Phys. Rev. B* **94**, 235451 (2016).
- [32] K. Takase, Y. Ashikawa, G. Zhang, K. Tateno, and S. Sasaki, *Sci. Rep.* **7**, 930 (2017).
- [33] O. Wunnicke, *Appl. Phys. Lett.* **89**, 083102 (2006).
- [34] A. C. Ford, J. C. Ho, Y.-L. Chueh, Y.-C. Tseng, Z. Fan, J. Guo, J. Bokor, and A. Javey, *Nano Lett.* **9**, 360 (2009).
- [35] S. Ghatak, A. N. Pal, and A. Ghosh, *ACS Nano* **5**, 7707 (2011).
- [36] A. Ayari, E. Cobas, O. Ogundadegbe, and M. S. Fuhrer, *J. Appl. Phys.* **101**, 014507 (2007).
- [37] K. Nomura and A. H. MacDonald, *Phys. Rev. Lett.* **96**, 256602 (2006).
- [38] S. Das Sarma, S. Adam, E. H. Hwang, and E. Rossi, *Rev. Mod. Phys.* **83**, 407 (2011).
- [39] Y. M. Sirenko and P. Vasilopoulos, *Phys. Rev. B* **46**, 1611 (1992).
- [40] S. Lyo, *Phys. Rev. B* **68**, 045310 (2003).
- [41] S. M. Badalyan and A. P. Jauho, *Phys. Rev. Res.* **2**, 013086 (2020).
- [42] B. N. Narozhny and A. Levchenko, *Rev. Mod. Phys.* **88**, 025003 (2016).
- [43] A. Lucas and K. C. Fong, *J. Phys. Condens. Matter* **30**, 053001 (2018).
- [44] L. Wang, I. Meric, P. Huang, Q. Gao, Y. Gao, H. Tran, T. Taniguchi, K. Watanabe, L. Campos, D. Muller *et al.*, *Science* **342**, 614 (2013).
- [45] F. Pizzocchero, L. Gammelgaard, B. S. Jessen, J. M. Caridad, L. Wang, J. Hone, P. Bøggild, and T. J. Booth, *Nat. Commun.* **7**, 11894 (2016).
- [46] W.-K. Tse, Ben Yu-Kuang Hu, and S. Das Sarma, *Phys. Rev. B* **76**, 081401(R) (2007).
- [47] B. N. Narozhny, M. Titov, I. V. Gornyi, and P. M. Ostrovsky, *Phys. Rev. B* **85**, 195421 (2012).
- [48] M. I. Katsnelson, *Phys. Rev. B* **84**, 041407(R) (2011).
- [49] N. Peres, J. L. Dos Santos, and A. C. Neto, *Europhys. Lett.* **95**, 18001 (2011).
- [50] Y. Xiong, H. Tang, X. Wang, Y. Zhao, Q. Fu, J. Yang, and D. Xu, *Sci. Rep.* **7**, 13252 (2017).
- [51] F. C. Wellstood, C. Urbina, and J. Clarke, *Phys. Rev. B* **49**, 5942 (1994).
- [52] S. K. Srivastav, M. R. Sahu, K. Watanabe, T. Taniguchi, S. Banerjee, and A. Das, *Sci. Adv.* **5**, eaaw5798 (2019).